Journal of Orthopaedic Surgery and Research

RESEARCH ARTICLE

Open Access

Validation and the role of PDK4 relevant to ferroptosis in degenerative lumbar disc disease

Wenhao Chen[1,2†], Wanliang Yang[1,2], Bin Meng[1,2], Xingkun Wang[1,2], Heng Duan[1,2], Qian Xu[1,2] and Hao Li[1*]

Abstract

Background Ferroptosis was involved in the pathogenesis of intervertebral disc degeneration (IVDD). However, the exact mechanism of IVDD associated with ferroptosis still required deeper studies.

Method The differentially expressed genes (DEGs) in rat lumbar disc tissue between the control and IVDD group treated with IL-1β were detected by RNA sequencing (RNA-seq). Gene Ontology (GO) and Kyoto Encyclopedia of Genes and Genomes (KEGG) enrichment analysis were performed on DEGs. We further screened the differential expressed ferroptosis-related genes (DEFRGs). Besides, a protein-protein interaction (PPI) network of DEFRGs was constructed by STRING database. The Cytoscape database identified significant modules and the hub genes. The loss function of PDK4 by siRNA inference was investigated in NPCs by CCK8 assay, ELISA assay, and the analysis of ferroptosis indicators.

Result DEGs were identified using RNA-seq. KEGG pathway analysis showed that these genes were mainly involved in Parkinson's disease, oxytocin signaling pathway, calcium ion signaling pathway, AMPK signaling pathway, and glucagon signaling pathway. Eight hub genes (including LDHA, PKM, EP300, EGFR, EGLN1, SCD, PDK4, and FABP4) were found by the PPI network and Cytoscape on a total of 25 ferroptosis-related genes that were identified in rat lumbar disc tissue after IVDD treatment. PDK4 silencing promoted NPCS proliferation, decreased the levels of the proinflammatory factors, and suppressed ferroptosis.

Conclusion The study suggested the potential roles of ferroptosis-related genes in IVDD and further revealed the role of PDK4 in the progression of IVDD.

Keywords Intervertebral disc degeneration, Pyruvate dehydrogenase kinase isozyme 4, RNA-sequencing, Ferroptosis, Hub gene

[†]Wenhao Chen is the first author.

*Correspondence:
Hao Li
hal@email.sdu.edu.cn
[1]Department of Orthopaedics, Qilu Hospital of Shandong University, No.107, Wenhuaxi Road, Lixia District, Jinan, Shandong Province 250012, China
[2]Cheeloo College of Medicine, Shandong University, No.107, Wenhuaxi Road, Lixia District, Jinan, Shandong Province 250012, China

Introduction

IVDD is the basis of various types of disc diseases, which is the predominant root cause leading to low back pain, one of the most common symptoms, with a high rate of disability, leading to a huge economic cost worldwide [1–3]. The nucleus pulposus (NP) is part of the disc structure between two cartilaginous plates and the annulus fibrosus (AF), the degradation of which could lead to a suite of pathological responses, such as ferroptosis, proinflammatory cytokines release (such as Interleukin (IL)-1β, IL-6, tumor necrosis factor (TNF)-α, and oxidative stress [4–7]. Interleukins are the main factors leading to inflammatory response in intervertebral disc tissues, playing an important role in IVDD [8]. The studies have shown that IL-1β can induce the high expression of matrix metalloproteinases in normal intervertebral disc and reduce the expression of tissue metalloproteinase inhibitors, thus disrupting the balance of intervertebral disc extracellular matrix decomposition and metabolism and accelerating the progression of IVDD.

Ferroptosis is a form of regulatory cell death mainly characterized by iron-dependent extensive lipid peroxidation, which is different from other forms of cell death in terms of cell morphology, biochemical characteristics, and genetics [9]. Emerging evidence reports the potential therapeutic effects of targeting ferroptosis against IVDD, which is found to be involved in the pathogenesis of IVDD [5, 6, 10]. Thus, there is a potential clinical value in developing a novel therapeutic strategy based on targeting ferroptosis for IVDD intervention, which prompts us to perform a deeper investigation on the pathogenesis of IVDD related to ferroptosis.

Pyruvate dehydrogenase complex (PDC) is a multienzyme complex located in the mitochondrial matrix that catalyzes oxidative decarboxylation of pyruvate and provides acetyl-CoA and NADH for tricarboxylic acid cycling and lipid biosynthesis, the activity of which is regulated by phosphorylation of its serine residues of E1α, which is modulated by dehydrogenase kinase (PDK). PDK4 is reported to be able to prevent ferroptosis by suppressing pyruvate oxidation and subsequent fatty acid synthesis and lipid peroxidation [11]. In this work, our objective was to investigate the DEGs in the rat model of IVDD and screen out DEFRGs, thereby identifying and verifying the hub genes in IVDD.

Method

IVDD rat model

Twelve Sprague Dawley rats (male, age: 8–10 weeks, weight: 220 ± 10 g, SPF, Beijing, China) were fed in a specific-pathogen free animal laboratory (humidity: 60-65%, temperature: 22–25℃) with 12 h light/12 dark cycle and felt free to get access to food and water. The rats were randomly divided into two groups, namely, the control group and the IVDD model group. The rats in the IVDD group were anesthetized by intraperitoneal injection of 2% (wt/vol) pentobarbital and then injected with 100 ng IL-1β into the Lumbar L5-6 position. To prevent inflammation, the rats were given intramuscular injection of 40 mg/kg penicillin and intragastric administration of 10 mg/kg acetylamin. After 2 weeks, magnetic resonance imaging (MRI) was performed. After 4 weeks, the rats were sacrificed by decapitation to collect lumbar disc tissue and blood. The experiment was reviewed and approved by the Institutional Animal Care and Use Committee of our hospital.

Identification of differentially expressed genes (DEGs)

Deseq2 package (1.34.0) was employed to identify DEGs in intervertebral disc tissue after IVDD treatment, which was characterized by $P < 0.05$ and $|\log2\text{-FoldChange}| > 1$. The heatmap was generated to visualize DEGs using the ggplots2 package.

Gene ontology and pathway enrichment analyses

The biological function of significant DEGs was analyzed through enrichment analysis of GO by the clusterProfiler package (4.2.2). The analysis of KEGG pathway for significant DEGs was performed using the clusterProfiler package (4.2.2) and the ggplot2 package (3.3.6) in R studio.

Identification of DEFRGs

GeneCards was used to extract ferroptosis-related genes (FRGs, Version 5.9, https://www.Genecards.org/). FRGs were overlapped with DEGs to obtain the intersections for further PPI analysis.

PPI Network, Module analysis and analysis of the Hub Genes

Search Tool for the Retrieval of Interacting Genes (STRING) database (version 11.5, https://cn.string-db.org/) was used to construct a PPI network to find out the potential interaction relationship between overlapped DEGs-encoded proteins. The threshold value was set by a required interaction score of 0.15. Next, the Cytoscape software (3.9.0) was used to construct the PPI network of overlapped DEGs. The significant PPI network modules were screened out using the Molecular Complex Detection (MCODE) plug-in. The hub genes were identified with the CytoHubba plug-in of Cytoscape by calculating eight different algorithms (MCC, DMNC, MNC, degree, closeness, radiality, stress, and EPC).

Hematoxylin-eosin staining (HE) staining

The frozen slices of lumbar intervertebral disc tissue were fixed with acetone at 20℃ for 10 min, rinsed in tap water at room temperature for 1–2 min, and then stained in

hematoxylin for 5 min. Next, the sections were immersed into acid alcohol for 1–3 s and then washed with water for 15 min. Subsequently, the sections were immersed into eosin for 1 min, followed by gradient dehydration in 80%, 95%, and 100% alcohol for 2 min sequentially, and xylene for 2 min. The sections were blocked with neutral balsam and observed under a light microscope.

TUNEL staining

At room temperature, paraffin tissue sections of lumbar intervertebral disc tissue were soaked in xylene for 5 min and replaced with new xylene for another 5 min to remove the paraffin completely. Next, following being immersed into 100% ethanol for 5 min and then into new 100% ethanol for another 5 min, the sections were soaked in gradient ethanol (90, 80, 70%) sequentially. Subsequently, 20 μg/ml Protease K was added into the sections for incubation for 20 min. The apoptosis of the lumbar intervertebral disc tissue was evaluated using a TUNEL kit (cat.no C1086, Beyotime Biotechnology, Shanghai, China) according to the manufacturer's protocol. 50 μL TUNEL solution was added to sections for incubation for 60 min at 37℃. The apoptosis was observed under a fluorescence microscope.

Immunohistochemistry (IHC)

The paraffin-embedded lumbar intervertebral disc tissue sections were deparaffinized, rehydrated, and subjected to antigen retrieval by high-pressure boiling in citrate buffer (pH 6.0) for 2 min. To block non-specific binding, sections were blocked with goat serum (Sigma-Aldrich, St. Louis, Missouri, USA), then incubated at 4 °C overnight with anti-PDK4 antibody (1:250, Proteintech, Rosemont, Illinois, USA). After staining with diaminobenzidine for 2 min and counterstaining with hematoxylin, the sections were observed under a microscope.

ELISA assay

The collected blood from rats was centrifuged at 3500 r/min at 4℃ for 20 min to obtain the supernatant. The supernatant of the cultured NPC cells was collected and centrifuged at 3000 r/min to obtain the supernatant. Following the manufacturer's guidance of ELISA kit (IL-18, cat.no P1555; IL-1β, cat.no PI303; TNF-α, cat.no PT516, Beyotime Biotechnology, Shanghai, China), the levels of IL-18, IL-1β, and TNF-α were evaluated by the detection of the absorbance at 450 nm with a microplate reader (Thermo Fisher Scientific, Pittsburgh, PA, USA).

RNA-sequencing

The rat intervertebral disc tissues from the control and IVDD were collected, separately. RNA extraction was performed using MasterPure™ Complete DNA and RNA Purification Kit MasterPure™ (MC85200, Epicentre, Madison, WI, Madison), followed by the determination of RNA concentration and purity by Nanodrop2000. RNA integrity number (RIN) was assessed by agarose gel electrophoresis and RIN was determined by Agilent 2100. Raw RNA sequencing required quality control (QC) on the raw reads to evaluate the suitability of the sequencing for subsequent analysis. RNA sequencing was performed on Illumina HiSeq using Next-Generation Sequencing (NGS).

NPC culture and transfection

Rat nucleus pulposus cells (NPC, Procell Life Science&Technology Co., Ltd, Wuhan, China) were cultured in DMEM/F12 medium at 37℃ with 5% CO_2, containing 10% fetal bovine serum, 1% streptomycin, and 1% penicillin (Hyclone, USA). NPCs were transfected with siPDK4 or its negative control siNC using lipo2000 (Invitrogen) according to the manufacturer's guidance. After 4–6 h, NPCs were treated with 10 μg/L IL-1β for 24 h for further experiments.

CCK-8 assay

The NPC proliferation of each group was detected by CCK-8 kit at 0 h, 24 h, 48 h, and 72 h (Abcam, England). The cells (200 μg/ml) were seeded into 96-well plates at 37℃ with 5% CO_2 for 24 h, 48 h, or 72 h. Then, 10 μL CCK-8 solution was added for incubation with cells for 2 h and the absorbance was measured at 450 nm using a microplate reader (Thermo Fisher Scientific).

Determination of malondialdehyde (MDA), superoxide dismutase (SOD) and glutathione (GSH)

The MDA and GSH levels, and SOD activity for NPC were measured using Malondialdehyde (MDA) colorimetric assay kit (cat.no.E-BC-K028-M, Elabscience, Wuhan, China), reduced glutathione (GSH) colorimetric assay kit (cat.no.E-BC-K030-M) and total superoxide Dismutase (T-SOD) activity assay kit (WST-1 Method, cat.no.E-BC-K020-M) according to the manufacturer's guidance.

Iron ion concentration determination

The iron determination in the NPC was determined using an Iron determination kit(colorimetry) (cat.no #K390-100BioVision.Inc) and the absorbance was measured at 593 nm using a microplate reader (Thermo Fisher Scientific).

RNA extraction and quantitative real-time RT-PCR

Total RNAs from NPCs were extracted using TRIZOL reagent, 5 μL of which was diluted 20 times with RNase-free Water. After the concentrations and purity of RNA were evaluated using an ultraviolet spectrophotometer, the RNA was reversed into complementary DNA

(cDNA), which then was used to perform Real-Time fluorescence quantitative PCR in ABI7500 quantitative PCR instrument (Applied Biosystems, USA). The PCR conditions contained pre-denaturation for 5 min at 95℃ and 40 cycles of denaturation for 10 s at 95℃, annealing for 30 s at 60℃. The relative RNA levels were evaluated by $2^{-\Delta\Delta Ct}$ method The sequence of primers (TaKaRa, Japan) used in this study is shown in Table 1.

Western blotting assay

After transfection for 48 h, NPCs were collected and lysed with RIPA Lysis solution (Beyotime technology, Shanghai, China). Then, the proteins were separated by the technology of SDS-PAGE and transferred into the PVDF membrane. Next, the membrane was blocked with 5%-TBST nonfat milk for 2 h at room temperature and incubated with the primary antibodies (anti-FTH1, cat.no ab183781, the dilution of 1:1000; anti-GPX4, cat. no ab125066, the dilution of 1:5000. anti-β-actin, cat. no ab6276, the dilution of 1:5000, abcam, England) (anti-ACLS4, cat.no PAB25681, the dilution of 1:1000, Amylet Scientific) overnight at 4℃. Then, the membrane was washed with TBST and incubated with secondary antibodies (horseradish peroxidase-conjugated Goat Anti-Rabbit IgG, the dilution of 1;5000, CWBIO, Beijing, China) for 2 h at room temperature. After the visualization of protein bands using enhanced chemiluminescence (cat.no 34095, Thermo Fisher Scientific), the protein levels were analyzed using the ChemiDoc Touch Imaging System (Bio-Rad). β-actin was used as an internal reference.

Table 1 The primer sequences

Genes	Sequences (5′-3′)
GAPDH-F	CTCATGACCACAGTCCATGC
GAPDH-R	TTCAGCTCTGGGATGACCTT
LDHA-F	GTGGAGTGGTGTGAATGTCG
LDHA-R	TTATGCTCTCGGCCAAGTCT
PKM-F	CTGCAGGTGAAGGAGAAAGG
PKM-R	CTCCCAGGACCTTCCTAACC
EGLN1-F	TACAGGATAAACGGCCGAAC
EGLN1-R	TTGGGTTCAATGTCAGCAAA
FABP4-F	TGAAATCACCCCAGATGACA
FABP4-R	TCACGCCTTTCATGACACAT
PDK4-1-F	CCTTTGGCTGGTTTTGGTTA
PDK4-2-R	CACCAGTCATCAGCCTCAGA
PDK4-2-F	GTTACGGCTTGCCGATTTCC
PDK4-2-R	CACTGCCGTAGACCCACTTT
PDK4-3-F	GGTTACGGCTTGCCGATTTC
PDK4-3-R	TAAAGTGCCAGGCGAGATCC
EGFR-F	ACCGTGGAGAGAATCCCTTT
EGFR-R	TTGTTGCTAAATCGCACAGC
EP300-F	CCTTCTCCTCGACCACAGTC
EP300-R	CGAGCTGTGAAAGCATTGAA
SCD-F	TCCTGCTCATGTGCTTCATC
SCD-R	GGATGTTCTCCCGAGATTGA

Statistical analysis

The experimental data were shown as mean ± standard deviation (SD) and analyzed by GraphPad Prism 8.0 statistical software. Comparison between two groups was performed by t-test and comparison among multiple groups was carried out by One-Way ANOVA analysis of variance, followed by Tukey's hoc test. $P < 0.05$ was considered as statistically significant.

Results

The establishment of IVDD rat model

First, a model of intervertebral disc degeneration was constructed in SD rats. The MRI results showed that intervertebral disc degeneration was seen in rats in the IVDD group (Fig. 1A), leading to narrowing of the intervertebral space (As shown by the white arrow). Similar results were also seen from HE staining for lumbar intervertebral disc tissue. The control group showed the arranged annulus fibrosus without inflammatory cell infiltration. However, the inflammatory cells were obviously increased, and disordered annulus were observed in the IVDD group (Fig. 1B). TUNEL results showed that there was obvious apoptosis in the IVDD group relative to control (Fig. 1C). Cytokines play an important role in the occurrence and deterioration of IVDD with various pathologic processes such as inflammation, apoptosis, and oxidative stress [12, 13]. As shown in Fig. 1D, the levels of IL-1β, TNF-α, and IL-18 in the IVDD group were significantly higher than those in the control group.

Identification of DEGs

In our work, we identified 723 DEGs with 487 genes upregulation and 236 downregulation in lumbar intervertebral disc tissue of IVDD rats (Fig. 2A). Expression levels of 723 DEGs were shown in the heatmap (Fig. 2B). Among 723 DEGs, the top 20 significantly up-regulated DEGs and the top 20 significantly down-regulated DEGs were listed in Table 2.

GO and KEGG pathway enrichment analysis of DEGs

To analyze the function and pathway of DEGs, GO and KEGG pathway enrichment analyses were performed. GO analysis indicated that DEGs were mainly involved in muscle structure development, muscle cell differentiation, striated muscle cell differentiation, muscle system processes, and muscle contraction in biological process (BP), and enriched in cytoskeletal protein binding, actin binding and muscle structural components in molecular function (MF), and contractile fibers, myofibril, sarcomere in cell component (CC) (Fig. 3A and B). KEGG pathway analysis showed that DEGs were mainly

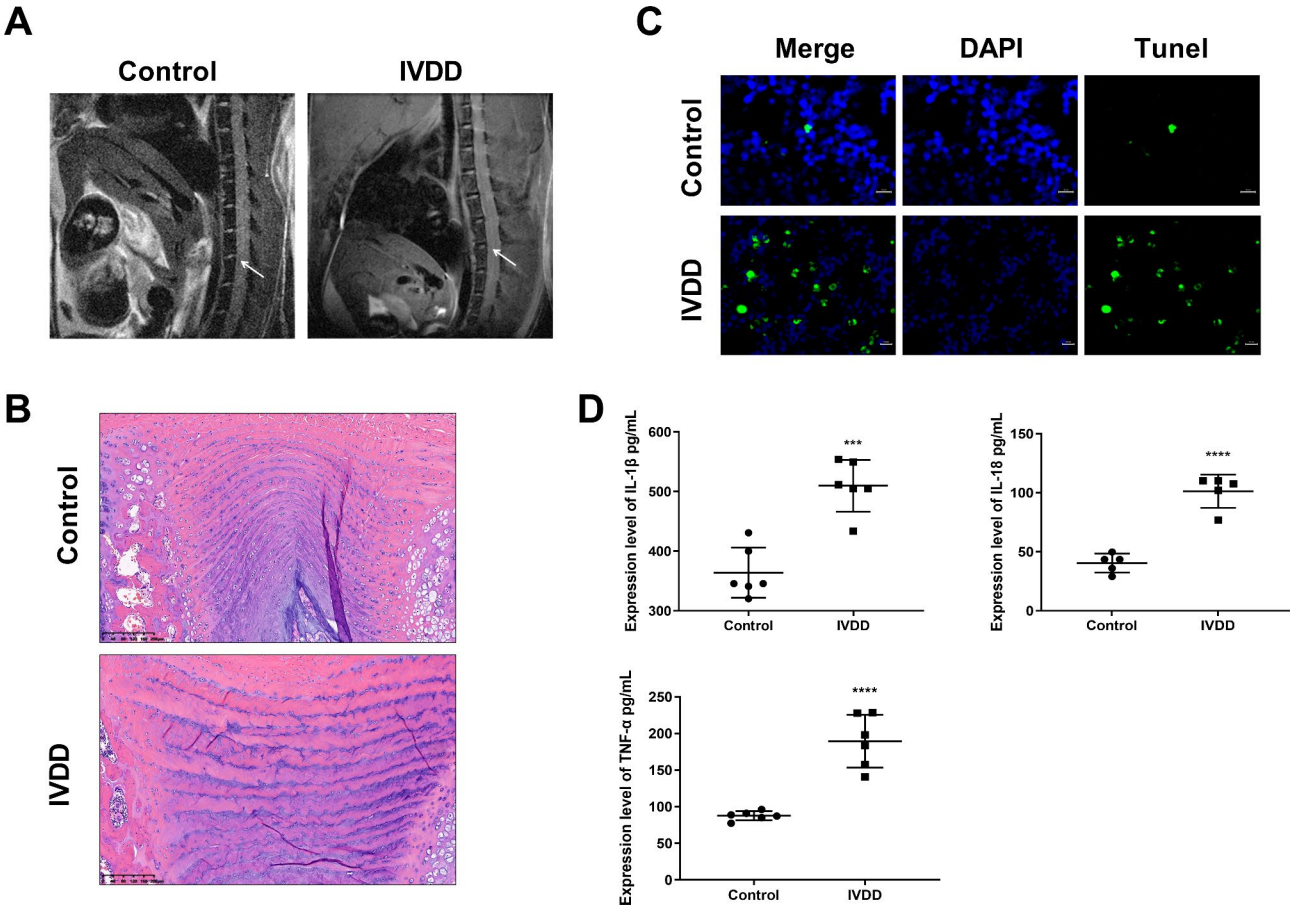

Fig. 1 Rat IVDD model was successfully established. **A** The magnetic resonance imaging. **B** The representative mages for HE staining of lumbar intervertebral disc tissue (Magnification: 10×, scale: 200 μm). **C** TUNEL staining. **D** The expression levels of IL-1β, TNF-α and IL-18 by ELISA analysis. $^{***}P < 0.001$ vs. Control. IVDD: intervertebral disc degeneration

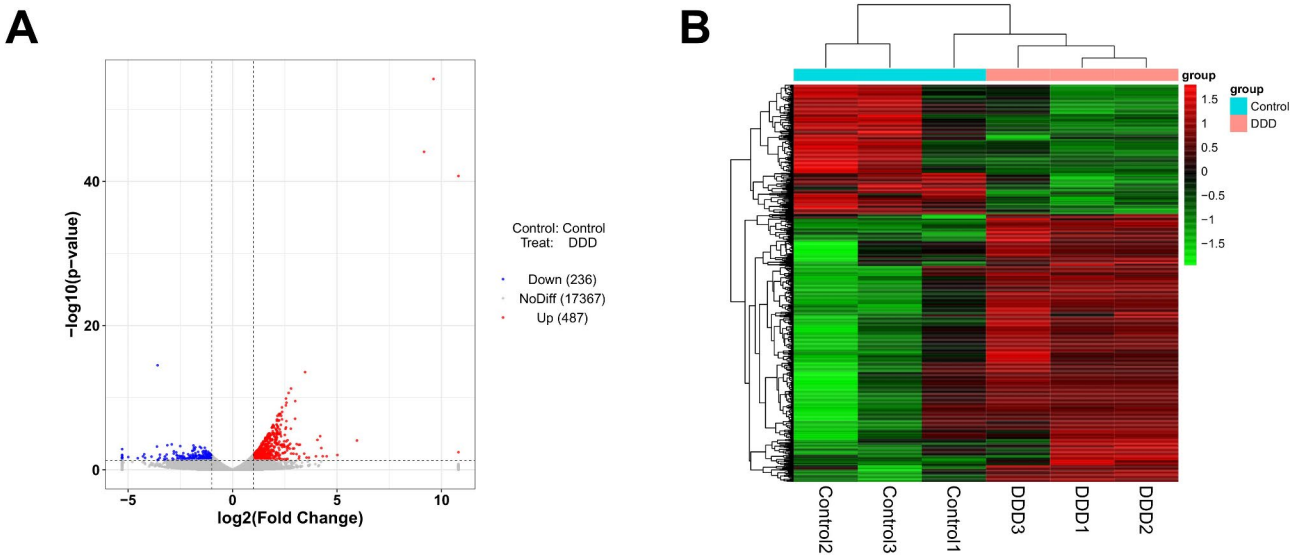

Fig. 2 Identification of DEGs after IVDD induction. **A** Volcano Plot of DEGs after IVDD treatment. **B** Heatmap of DEGs. DEGs: differentially expressed genes; IVDD: intervertebral disc degeneration

Table 2 Differentially expressed genes

PG.Genes	Description	log2fc	pval	padj	Up/Down
Kdm5d	lysine demethylase 5D	10.805	0.000	0.000	Up
Ddx3	DEAD (Asp-Glu-Ala-Asp) box polypeptide 3	9.612	0.000	0.000	Up
Eif2s3y	eukaryotic translation initiation factor 2, subunit 3	9.162	0.000	0.000	Up
Acsm5	acyl-CoA synthetase medium-chain family member 5	5.952	0.000	0.014	Up
Klra1	killer cell lectin-like receptor, subfamily A, member 1	5.015	0.009	0.425	Up
Try5	trypsin 5	4.504	0.014	0.531	Up
Rad21l1	RAD21 cohesin complex component like 1	4.314	0.013	0.528	Up
Ubxn10	UBX domain protein 10	4.247	0.001	0.087	Up
Lrrc30	leucine rich repeat containing 30	4.192	0.000	0.005	Up
Lep	leptin	4.060	0.000	0.012	Up
Fpr3	formyl peptide receptor 3	3.991	0.014	0.531	Up
Sirpd	signal-regulatory protein delta	3.654	0.021	0.670	Up
Sbk3	SH3 domain binding kinase family, member 3	3.541	0.020	0.668	Up
Asb9	ankyrin repeat and SOCS box-containing 9	3.471	0.000	0.000	Up
AABR07060994.1	-	3.427	0.006	0.325	Up
Smtnl2	smoothelin-like 2	3.227	0.000	0.039	Up
H3f3c	H3 histone family member 3 C	3.192	0.014	0.545	Up
Ces1a	carboxylesterase 1 A	3.176	0.028	0.768	Up
Myoz1	myozenin 1	3.163	0.000	0.040	Up
Myf6 Tuba1c	myogenic factor 6 tubulin, alpha 1 C	3.065	0.000 0.013	0.036 0.521	Up
Elf4	E74 like ETS transcription factor 4	-1.003	0.025	0.734	Down
Arhgap28	Rho GTPase activating protein 28	-1.006	0.044	0.907	Down
RGD1566265	similar to RIKEN cDNA 2610002M06	-1.007	0.041	0.880	Down
Vangl2	VANGL planar cell polarity protein 2	-1.008	0.047	0.931	Down
Mcph1	microcephalin 1	-1.012	0.030	0.785	Down
Cds1	CDP-diacylglycerol synthase 1	-1.015	0.046	0.921	Down
Zfp518b	zinc finger protein 518B	-1.015	0.038	0.856	Down
Pltp	phospholipid transfer protein	-1.018	0.009	0.414	Down
Elmo1	engulfment and cell motility 1	-1.018	0.009	0.435	Down
Birc6	baculoviral IAP repeat-containing 6	-1.022	0.012	0.504	Down
Tmem104	transmembrane protein 104	-1.022	0.032	0.806	Down
Ep300	E1A binding protein p300	-1.026	0.023	0.716	Down
Ppp1r16b	protein phosphatase 1, regulatory subunit 16B	-1.027	0.048	0.935	Down
Gas1	growth arrest-specific 1	-1.027	0.040	0.876	Down
Gabpb2	GA binding protein transcription factor subunit beta 2	-1.028	0.025	0.745	Down
LOC100910732	serine/threonine-protein kinase PAK 2-like	-1.033	0.027	0.765	Down
Cd274	CD274 molecule	-1.039	0.044	0.901	Down
Extl3	exostosin-like glycosyltransferase 3	-1.040	0.011	0.478	Down
Uhmk1	U2AF homology motif kinase 1	-1.041	0.011	0.479	Down
Rbl1	RB transcriptional corepressor like 1	-1.041			Down

involved in Parkinson's disease, oxytocin signaling pathway, calcium ion signaling pathway, AMPK signaling pathway, and glucagon signaling pathway (Fig. 3C and D).

PPI analysis of DEFRGs and the identification of hub genes

Among the screened DEGs by RNA-seq in lumbar intervertebral disc tissue of IVDD rats, 25 genes were identified to be associated with ferroptosis as shown in. The results from the PPI network of DEFRGs with 24 nodes and 32 edges were constructed by STRING and were presented by Cytoscape. MCODE plug-in of Cytoscape revealed two significant modules and 8 hub genes were found including lactate dehydrogenase A (LDHA), Pyruvate kinase muscle (PKM), E1A binding protein P300 (EP300), epidermal growth factor receptor (EGFR), Egg-Laying Defective Nine 1(EGLN1), Stearoyl-coenzyme A desaturase (SCD), PDK4, and Fatty Acid Biding Protein-4 (FABP4) (Fig. 4A-B).

Validation of hub genes expression in IVDD model in vitro

IVDD model was constructed in rat NPCs with IL-1β. The results from the qRT-PCR assay demonstrated that the expression of LDHA, PKM, EGLN1, FABP4, and PDK4 showed significant upregulation and EGFR, EP300, and SCD levels exhibited significant downregulation in the IL-1β-induced NPCs compared with the control group without IL-1β treatment (Fig. 5A). Based on the literature review, Hub gene PDK4 was selected for further mechanism exploration associated with IVDD pathogenesis in subsequent in vitro. IHC staining further validated that PDK4 expression was elevated in the IVDD rat model compared to the control group (Fig. 5B).

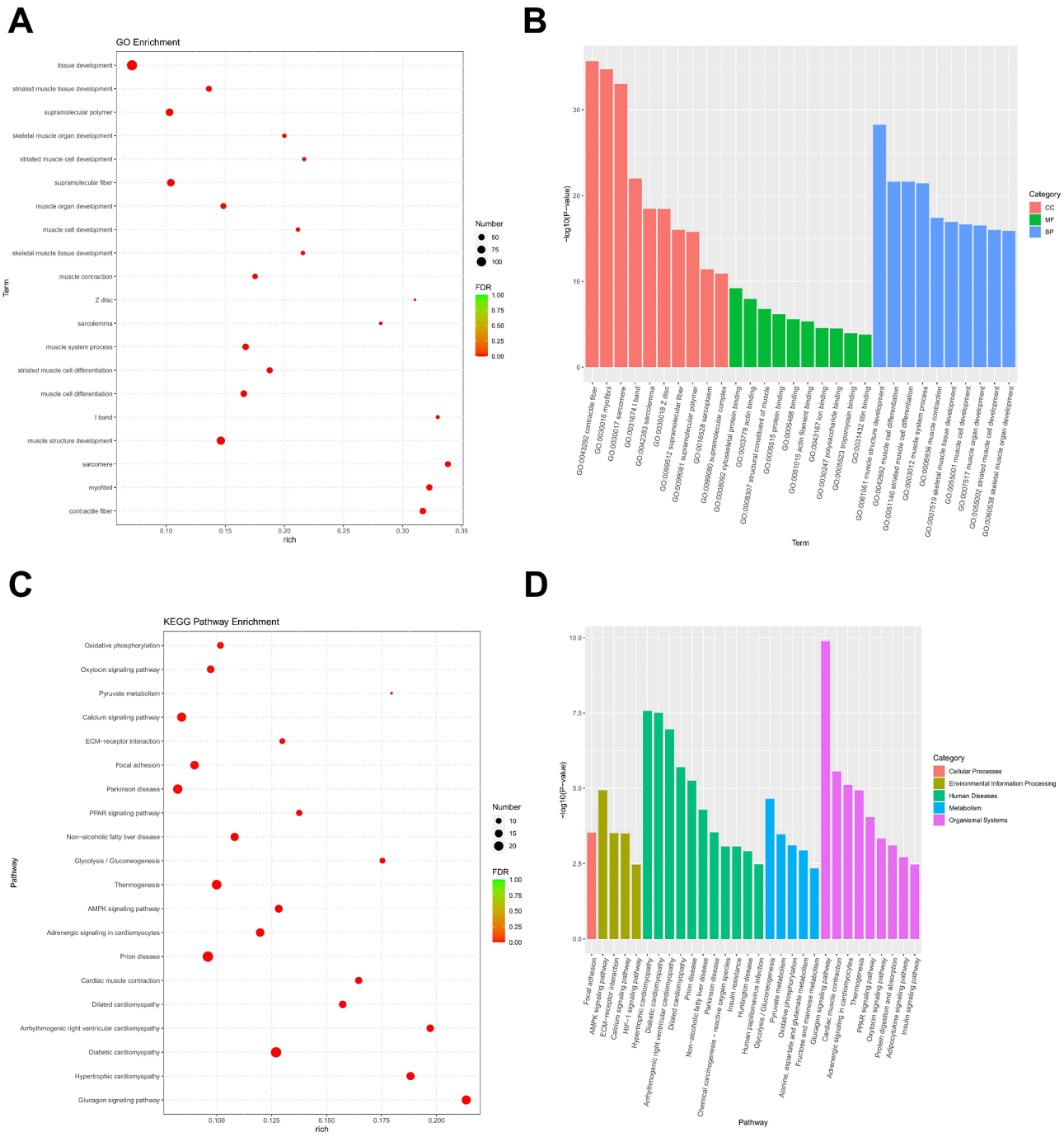

Fig. 3 Enrichment analysis of DEGs after IVDD. **A** The bubble chart for GO enrichment analysis. **B** The bar graph for GO enrichment analysis. **C** The bubble chart for KEGG enrichment analysis. **D** The bar graph for KEGG enrichment analysis. DEGs: differentially expressed genes; GO: gene ontology; KEGG: Kyoto Encyclopedia of Genes and Genomes

PDK4 silencing suppressed NPCs proliferation, inflammation and ferroptosis

To investigate the role of PDK4 in IVDD, PDK4 silencing was induced by constructing 3 siRNAs. As displayed in Fig. 6A, the effects of siPDK4-1 silencing PDK4 expression were superior to others including siPDK4-2 and siPDK4-3. Next, we focused on the effects of siPDK4-1 on proliferation and the expression of inflammatory factors in NPCs after IL-1β induction. PDK4 silencing significantly promoted NPCs proliferation (Fig. 6B) and decreased the levels of proinflammatory factors IL-18, IL-1β, and TNF-α (Fig. 6C). These findings indicate that PDK4 silencing could slow the IVDD progression and PDK4 could play a vital role in IVDD progression.

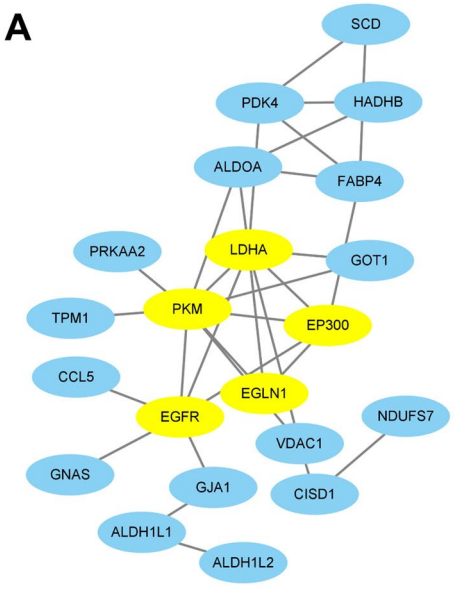

Fig. 4 The PPI analysis of DEFRGs. **A–B** Using the MCODE plugin of Cytoscape, two significant modules and 8 hub genes were identified. PPI: protein-protein interaction; DEFRGs: differential expressed ferroptosis-related genes; MCODE: Molecular Complex Detection

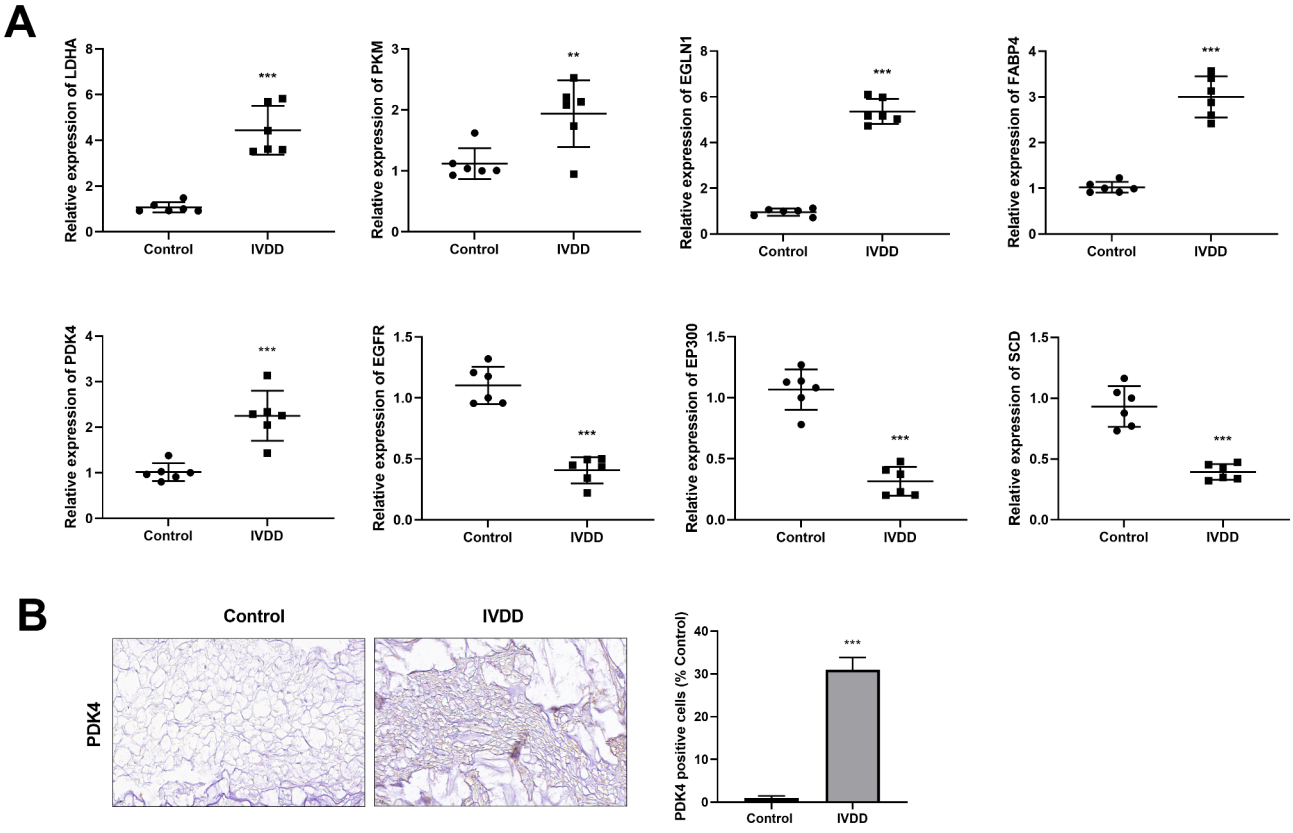

Fig. 5 Validation of the expression levels of hub genes. **A** QRT-PCR analysis of Hub genes, LDHA, PKM, EP300, EGFR, EGLN1, SCD, PDK4 and FABP4 in rat NPCS treated with IL-1β. **B** IHC was used to detect the expression level of PDK4 in the control and IVDD rat model group. (Magnification: 400×, Scale: 20 μm). $^{**}P < 0.01$, $^{***}P < 0.001$ vs. Control. LDHA: Lactate dehydrogenase A; PKM: Pyruvate kinase muscle; EP300: E1A binding protein P300; EGFR: epidermal growth factor receptor; EGLN1: Egg-Laying Defective Nine; SCD: Stearoyl-coenzyme A desaturase; PDK4: pyruvate dehydrogenase kinase isozyme 4; FABP4: Fatty Acid Biding Protein-4; IHC: immunohistochemistry

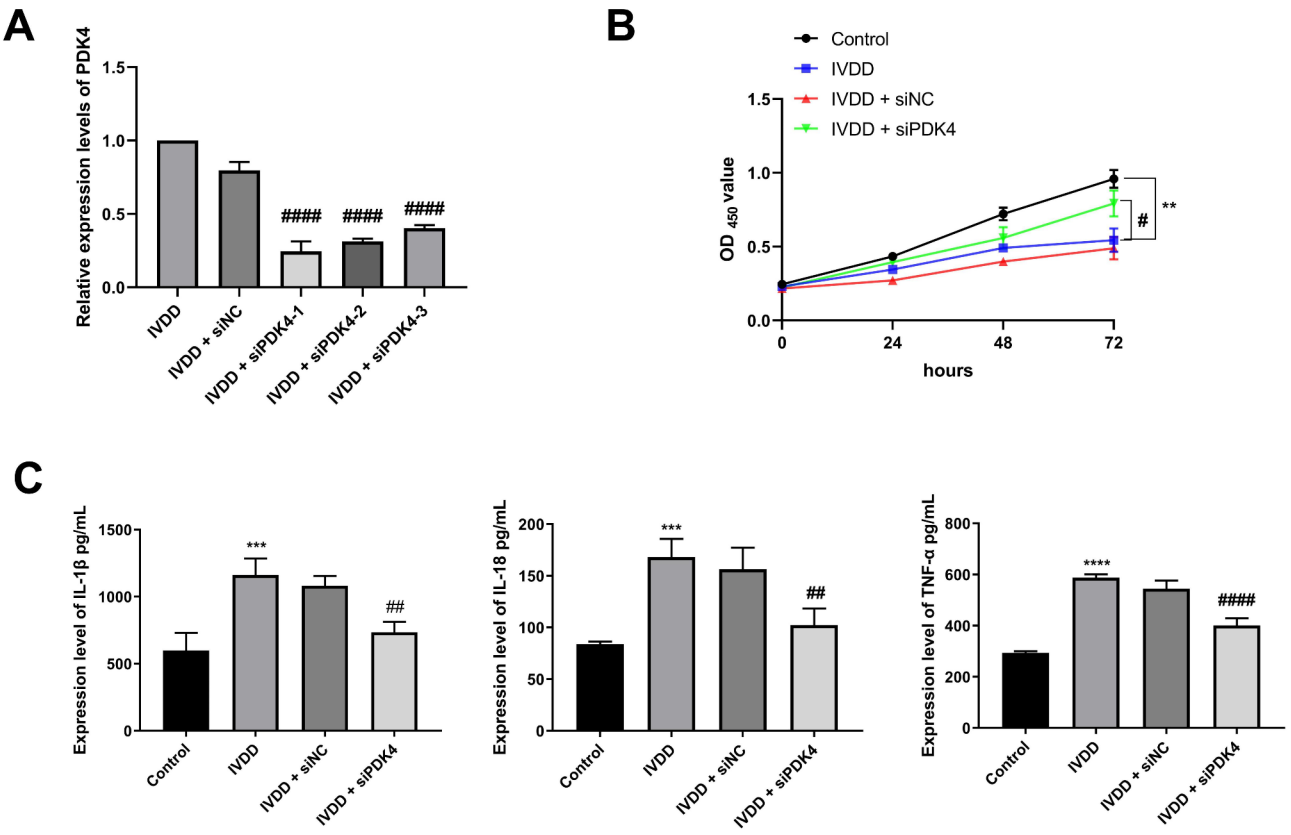

Fig. 6 PDK4 silencing promoted proliferation and suppressed inflammation in rat NPCs. **A** The transfection efficacy of siPDK4-1, -2 and – 3. **B** The analysis of rat NPCS proliferation by CCK8 assay. **C** The evaluation of IL-1β, TNF-α and IL-18 levels by ELISA assay. $^{**}P < 0.01$, $^{***}P < 0.001$ vs. Control; $^{\#}P < 0.05$, $^{\#\#}P < 0.01$, $^{\#\#\#}P < 0.001$ vs. IVDD + siNC

To further explore whether the potential mechanism of PDK4 involved in IVDD progression could be related to ferroptosis, the effects of PDK4 silencing on ferroptosis-associated indicators were detected in NPCs. Lipid peroxidation, GSH depletion, and iron accumulation are considered as the key events in ferroptosis [14–16]. The results showed that compared with the control group, there were significantly increased MDA and iron levels, and decreased SOD activity and GSH level in the IVDD group, which was significantly reversed by PDK4 silencing (Fig. 7A and B). GPX4 is a key regulator of ferroptosis, which could reduce the toxicity of lipid peroxides by its catalytic activity and maintain the homeostasis of the membrane lipid bilayer, thereby inhibiting ferroptosis [17, 18]. It was reported that factor inhibiting (HIF-1) inhibits ferroptosis by disrupting the iron autophagosome [19]. Acyl-CoA synthetase long-chain family member 4 (ACSL4) functions as a key enzyme regulating lipid composition, and promotes ferroptosis [20]. Western blot and qRT-PCR results showed that PDK4 silencing inhibited the expression of ACSL4 and upregulated the GPX4 and FTH1 expression levels (Fig. 7C and D). Thus, PDK4 was involved in ferroptosis in NPCS challenged with IL-1β, suggesting that the mechanism of PDK4 involved in IVDD could be associated with ferroptosis.

Discussion

In the present study, RNA-sq was performed to screen out DEGs in lumbar intervertebral disc tissue after IVDD induction, which was used to perform GO analysis and KEGG analysis, revealing the functional enrichment and pathway enrichment, respectively. Then, 8 hub genes were further screened through the PPI network and Cytoscape, and were verified in vitro, which provides new insights for exploring IVDD mechanism. In addition, the hub gene PDK4 was found to be involved in the IVDD progression and regulate ferroptosis, indicating the potential therapeutic role of targeting PDK4 in IVDD and providing a new research direction for studying the mechanism of IVDD.

Of the 25 DEFRGs, 8 genes including LDHA, PKM, EP300, EGFR, EGLN1, SCD, PDK4, and FABP4 were identified as hub genes. We observed the upregulation in LDHA mRNA levels in rat NPCs after IL-1β treatment compared with that in cells without IL-1β treatment, suggesting that it plays a role in IVDD. A report for NPCs found that LDHA is implicated in IVDD by modulating

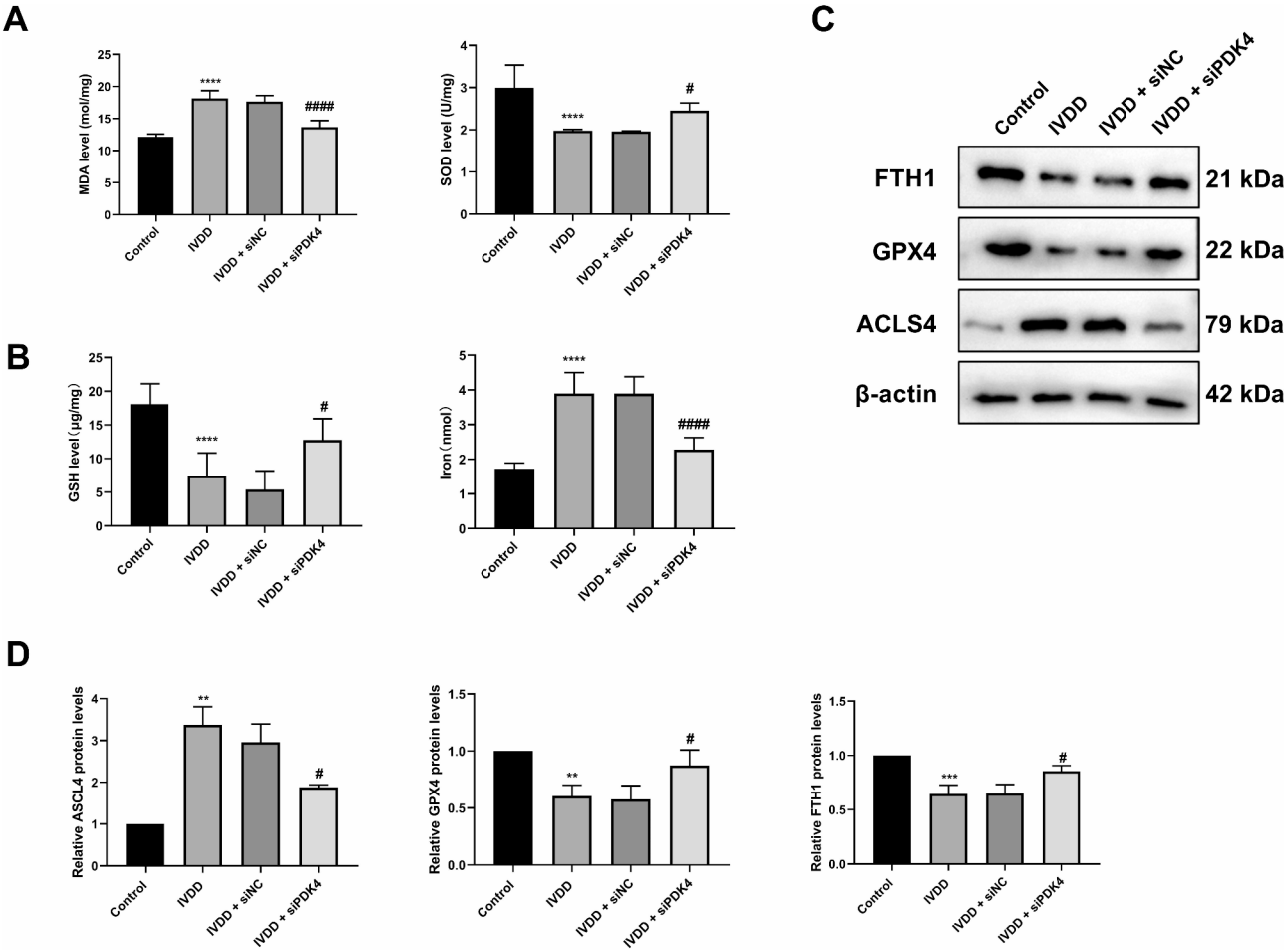

Fig. 7 PDK4 silencing suppressed ferroptosis in rat NPCS exposed to IL-1β. **A** The SOD activities and MDA levels. **B** The GSH levels and iron content. **C** Western blotting analysis of ACSL4, GPX4 and FTH1 protein. **D** The relative protein levels of ACSL4, GPX4 and FTH1 protein. $^{**}P < 0.01$, $^{***}P < 0.001$ vs. Control; $^{\#}P < 0.05$, $^{\#\#\#}P < 0.001$, vs. IVDD + siNC

glycolytic metabolism. In addition, the study also demonstrated that an upstream gene of LDHA, c-Myc was positively regulated by SIRT1, suggesting the potential regulatory role of LDHA in IVDD [21].

PKM isoforms, the key enzymes in the glycolytic pathway, participated in metabolism and proliferation [22]. PKM levels show upregulation in NPCs with IL-1β challenge. More attention is obtained for PKM on its non-canonical roles in tumorigenesis [23–25]. For IVDD, PKM2-JMJD5 axis independents of prolyl hydroxylase-3, functioning as a hypoxia inducible factor-1a cofactor, which is closely associated with NPCS degeneration [26]. EP300 mutations are observed in a variety of malignancies, which are found to be mainly involved in cancer progression, such as bladder cancer and diffuse large B-cell lymphoma [27, 28]. The mechanism of EP300 involved in cancer is investigated to function by modulating the enhancers of certain genes. With regard as the role of EP300 in IVDD, EP300 participates in IVDD by the modulation of miRNA [29]. Aberrant EGFR activation in human and rat IVDD and its depletion can influence the production of extracellular matrix and autophagy marker in IVDD mice. Moreover, its inhibition by gefitinib, an EGFR inhibitor, lowers the disc degenerating progression in patients, suggesting the therapeutic effects of targeting EGFR in IVDD [30]. EGLN1, an oxygen sensor, leads to the proteasomal degradation of hypoxia-inducible factor-1 α by catalyzing its prolyl hydroxylation, which is reported to be involved in tumor progression [31–33]. In addition, EGLN1 is involved in regulating ferroptosis by affecting the expression of lipid metabolic genes [34]. The studies for SCD mainly focus on metabolic syndrome, which is considered a potential target to control the progression of related metabolic diseases including type 2 diabetes, hepatic steatosis, and obesity [34, 35]. Additionally, SCD1 in cancer cells and FABP4 in tumor microenvironment dictate tumor resistance to ferroptosis, facilitating tumor growth. However, the effects of SCD, PDK4, and FABP4 relevant to IVDD have been less reported, which still requires more exploration in IVDD

since there were significant changes in SCD, PDK4, and FABP4 expression being found in the IVDD model in the present study.

Additionally, to further clarify the mechanism of hub genes in IVDD associated with ferroptosis and narrow the study, hub gene PDK4 was selected to perform a loss function experiment since the effects of PDK4 were reported in recent studies relevant to ferroptosis [11, 36]. The regulatory role of PDK4 in ferroptosis is identified as associated with pyruvate oxidation and fatty acid synthesis [11]. In our work, by performing PDK4 silencing assay in NPCs treated with IL-1β, NPCs degeneration was significantly lowered and the ferroptosis was suppressed by the analysis of ferroptosis markers, implying that there could be a connection between the mechanism of PDK4 on IVDD and ferroptosis, which still require more studies to reveal it. PDK4 attracted much attention since there was less research about the role of PDK4 in IVDD. PDK4 upregulation was thought to play a role in IVDD, which could have a relevant relation with ferroptosis.

However, this study also has some limitations. First, we identified 8 hub genes associated with ferroptosis but focused only on exploring the role of PDK4. The roles of the other genes in IVDD require further validation. Then, our in vitro experiments verified that PDK4 silencing could effectively promote proliferation, and suppress inflammation and ferroptosis; however, the absence of in vivo data, due to time and scientific limitations, necessitates our future studies to understand its function in IVDD comprehensively.

Conclusions

In summary, the study identified 487 genes up-regulated and 236 genes down-regulated by RNA-Seq analysis of transcriptome in lumbar intervertebral disc tissue in IVDD rats. A total of 25 ferroptosis-associated DEGs were identified, and 8 hub genes, including LDHA, PKM, EP300, EGFR, EGLN1, SCD, PDK4, and FABP4, could provide potential insights for further exploration of the pathogenesis of IVDD. We further identified the critical gene PDK4, playing a vital role in IDVV progression, this mechanism of which was considered to be closely related to the inhibition of ferroptosis. Findings from this work provide novel insights into the role of PDK4 in NPCs proliferation, inflammation, and ferroptosis, deserving deeper investigations into the underlying molecular mechanisms and potential therapeutic applications.

Supplementary Information

The online version contains supplementary material available at https://doi.org/10.1186/s13018-024-05293-8.

Supplementary Material 1

Supplementary Material 2

Supplementary Material 3

Supplementary Material 4

Supplementary Material 5

Supplementary Material 6

Supplementary Material 7

Supplementary Material 8

Acknowledgements
Not applicable.

Author contributions
Conceptualization, WHC&WLY; Methodology, WHC&WLY; Investigation, BM&XKW; Formal Analysis, BM&XKW; Writing - Original Draft, WHC&WLY; Writing - Review & Editing, HD, QX&HL. All authors took part in the experiment. All authors read and approved the final manuscript.

Funding
Not applicable.

Data availability
The data and materials supporting the findings of this study are available from the corresponding authors upon request.

Declarations

Ethics approval and consent to participate
The animal experiments were approved by the Qilu Hospital of Shandong University ethical committee in accordance with the ARRIVE guidelines.

Consent for publication
Not applicable.

Competing interests
The authors declare no competing interests.

Received: 2 September 2024 / Accepted: 18 November 2024
Published online: 10 January 2025

References

1. Cieza A, Causey K, Kamenov K, Hanson SW, Chatterji S, Vos T. Global estimates of the need for rehabilitation based on the Global Burden of Disease study 2019: a systematic analysis for the global burden of Disease Study 2019. Lancet. 2021;396(10267):2006–17.
2. Hartvigsen J, Hancock MJ, Kongsted A, Louw Q, Ferreira ML, Genevay S, et al. What low back pain is and why we need to pay attention. Lancet. 2018;391(10137):2356–67.
3. Dieleman JL, Cao J, Chapin A, Chen C, Li Z, Liu A, et al. US Health Care Spending by Payer and Health Condition, 1996–2016. JAMA. 2020;323(9):863–84.
4. Lyu FJ, Cui H, Pan H, Mc Cheung K, Cao X, Iatridis JC, et al. Painful intervertebral disc degeneration and inflammation: from laboratory evidence to clinical interventions. Bone Res. 2021;9(1):7.
5. Zhang Y, Han S, Kong M, Tu Q, Zhang L, Ma X. Single-cell RNA-seq analysis identifies unique chondrocyte subsets and reveals involvement of ferroptosis in human intervertebral disc degeneration. Osteoarthritis Cartilage. 2021;29(9):1324–34.
6. Lu S, Song Y, Luo R, Li S, Li G, Wang K, et al. Ferroportin-Dependent Iron Homeostasis protects against oxidative stress-Induced Nucleus Pulposus Cell Ferroptosis and ameliorates intervertebral disc degeneration in vivo. Oxid Med Cell Longev. 2021;2021:6670497.
7. Li Y, Pan D, Wang X, Huo Z, Wu X, Li J, et al. Silencing ATF3 might Delay TBHP-Induced intervertebral disc degeneration by repressing NPC Ferroptosis, apoptosis, and ECM degradation. Oxid Med Cell Longev. 2022;2022:4235126.

8. Sun HY, Hu KZ, Yin ZS. Inhibition of the p38-MAPK signaling pathway suppresses the apoptosis and expression of proinflammatory cytokines in human osteoarthritis chondrocytes. Cytokine. 2017;90:135–43.
9. Dixon SJ, Lemberg KM, Lamprecht MR, Skouta R, Zaitsev EM, Gleason CE, et al. Ferroptosis: an iron-dependent form of nonapoptotic cell death. Cell. 2012;149(5):1060–72.
10. Wang YG, Yu XJ, Qu YK, Lu R, Li MW, Xu HR et al. Ferrostatin-1 inhibits toll-like receptor 4/NF-kappaB signaling to alleviate intervertebral disc degeneration in rats. Am J Pathol. 2023.
11. Song X, Liu J, Kuang F, Chen X, Zeh HJ 3rd, Kang R, et al. PDK4 dictates metabolic resistance to ferroptosis by suppressing pyruvate oxidation and fatty acid synthesis. Cell Rep. 2021;34(8):108767.
12. Xia C, Zeng Z, Fang B, Tao M, Gu C, Zheng L, et al. Mesenchymal stem cell-derived exosomes ameliorate intervertebral disc degeneration via anti-oxidant and anti-inflammatory effects. Free Radic Biol Med. 2019;143:1–15.
13. Ma Z, Tang P, Dong W, Lu Y, Tan B, Zhou N, et al. SIRT1 alleviates IL-1β induced nucleus pulposus cells pyroptosis via mitophagy in intervertebral disc degeneration. Int Immunopharmacol. 2022;107:108671.
14. Imai H, Matsuoka M, Kumagai T, Sakamoto T, Koumura T. Lipid peroxidation-dependent cell death regulated by GPx4 and Ferroptosis. Curr Top Microbiol Immunol. 2017;403:143–70.
15. Latunde-Dada GO, Ferroptosis. Role of lipid peroxidation, iron and ferritinophagy. Biochim Biophys Acta Gen Subj. 2017;1861(8):1893–900.
16. Shui S, Zhao Z, Wang H, Conrad M, Liu G. Non-enzymatic lipid peroxidation initiated by photodynamic therapy drives a distinct ferroptosis-like cell death pathway. Redox Biol. 2021;45:102056.
17. Maru D, Hothi A, Bagariya C, Kumar A. Targeting ferroptosis pathways: a Novel Strategy for Cancer Therapy. Curr Cancer Drug Targets. 2022;22(3):234–44.
18. Wu Z, Khodade VS, Chauvin JR, Rodriguez D, Toscano JP, Pratt DA. Hydropersulfides inhibit lipid peroxidation and protect cells from Ferroptosis. J Am Chem Soc. 2022;144(34):15825–37.
19. Shan X, Lv ZY, Yin MJ, Chen J, Wang J, Wu QN. The Protective Effect of Cyanidin-3-Glucoside on Myocardial Ischemia-Reperfusion Injury through Ferroptosis. Oxid Med Cell Longev. 2021;2021:8880141.
20. Li Y, Feng D, Wang Z, Zhao Y, Sun R, Tian D, et al. Ischemia-induced ACSL4 activation contributes to ferroptosis-mediated tissue injury in intestinal ischemia/reperfusion. Cell Death Differ. 2019;26(11):2284–99.
21. Wu L, Shen J, Zhang X, Hu Z. LDHA-Mediated glycolytic metabolism in Nucleus Pulposus cells is a potential therapeutic target for intervertebral disc degeneration. Biomed Res Int. 2021;2021:9914417.
22. Demeter JB, Elshaarrawi A, Dowker-Key PD, Bettaieb A. The emerging role of PKM in keratinocyte homeostasis and pathophysiology. FEBS J. 2022.
23. Jiang J, Huang D, Jiang Y, Hou J, Tian M, Li J, et al. Lactate modulates Cellular Metabolism through histone lactylation-mediated gene expression in Non-small Cell Lung Cancer. Front Oncol. 2021;11:647559.
24. Ma WK, Voss DM, Scharner J, Costa ASH, Lin KT, Jeon HY, et al. ASO-Based PKM splice-switching therapy inhibits Hepatocellular Carcinoma Growth. Cancer Res. 2022;82(5):900–15.
25. Masoud GN, Li W. HIF-1α pathway: role, regulation and intervention for cancer therapy. Acta Pharm Sin B. 2015;5(5):378–89.
26. Schoepflin ZR, Silagi ES, Shapiro IM, Risbud MV. PHD3 is a transcriptional coactivator of HIF-1α in nucleus pulposus cells independent of the PKM2-JMJD5 axis. Faseb j. 2017;31(9):3831–47.
27. Zhu G, Pei L, Li Y, Gou X. EP300 mutation is associated with tumor mutation burden and promotes antitumor immunity in bladder cancer patients. Aging. 2020;12(3):2132–41.
28. Barretina J, Caponigro G, Stransky N, Venkatesan K, Margolin AA, Kim S, et al. The Cancer Cell Line Encyclopedia enables predictive modelling of anticancer drug sensitivity. Nature. 2012;483(7391):603–7.
29. Durbin AD, Wang T, Wimalasena VK, Zimmerman MW, Li D, Dharia NV, et al. EP300 selectively controls the enhancer Landscape of MYCN-Amplified Neuroblastoma. Cancer Discov. 2022;12(3):730–51.
30. Dong W, Liu J, Lv Y, Wang F, Liu T, Sun S, et al. miR-640 aggravates intervertebral disc degeneration via NF-kappaB and WNT signalling pathway. Cell Prolif. 2019;52(5):e12664.
31. Pan Z, Sun H, Xie B, Xia D, Zhang X, Yu D, et al. Therapeutic effects of gefitinib-encapsulated thermosensitive injectable hydrogel in intervertebral disc degeneration. Biomaterials. 2018;160:56–68.
32. Sun L, Wu C, Ming J, Guo E, Zhang W, Li L, et al. EGLN1 induces tumorigenesis and radioresistance in nasopharyngeal carcinoma by promoting ubiquitination of p53 in a hydroxylase-dependent manner. J Cancer. 2022;13(7):2061–73.
33. Tang J, Deng H, Wang Z, Zha H, Liao Q, Zhu C, et al. EGLN1 prolyl hydroxylation of hypoxia-induced transcription factor HIF1α is repressed by SET7-catalyzed lysine methylation. J Biol Chem. 2022;298(6):101961.
34. Brown JM, Rudel LL. Stearoyl-coenzyme A desaturase 1 inhibition and the metabolic syndrome: considerations for future drug discovery. Curr Opin Lipidol. 2010;21(3):192–7.
35. AM AL, Syed DN, Ntambi JM. Insights into Stearoyl-CoA Desaturase-1 regulation of systemic metabolism. Trends Endocrinol Metab. 2017;28(12):831–42.
36. Liu J, Kang R, Tang D. Metabolic checkpoint of ferroptosis resistance. Mol Cell Oncol. 2021;8(3):1901558.

Publisher's note